Trans-Window Panoramic Impasto for Online Tissue Deformation Recovery

Jiahe Chen[1], Etsuko Kobayashi[1], Ichiro Sakuma[1], Naoki Tomii[1](✉)

[1] School of Engineering, The University of Tokyo, Tokyo, Japan
naoki_tomii@bmpe.t.u-tokyo.ac.jp

Abstract. Deformation recovery from laparoscopic images benefits many downstream applications like robot planning, intraoperative navigation and surgical safety assessment. We define tissue deformation as time-variant surface structure and displacement. Besides, we also pay attention to the surface strain, which bridges the visual observation and the tissue biomechanical status, for which continuous pointwise surface mapping and tracking are necessary. Previous SLAM-based methods cannot cope with instrument-induced occlusion and severe scene deformation, while the neural field-based ones are offline and scene-specific, which hinders their application in continuous mapping. Moreover, neither approach meets the requirement of continuous pointwise tracking. To overcome these limitations, we assume a deformable environment and a movable window through which an observer depicts the environment's 3D structure on a canonical canvas as maps in a process named impasto. The observer performs panoramic impasto for the currently and previously observed 3D structure in a two-step online approach: optimization and fusion. The optimization of the maps compensates for the error in the observation of the structure and the tracking by preserving spatiotemporal smoothness, while the fusion is for merging the estimated and the newly observed maps by ensuring visibility. Experiments were conducted using ex vivo and in vivo stereo laparoscopic datasets where tool-tissue interaction occurs and large camera motion exists. Results demonstrate that the proposed online method is robust to instrument-induced occlusion, capable of estimating surface strain, and can continuously reconstruct and track surface points regardless of camera motion. Code is available at: https://github.com/bmpelab/trans_window_panoramic_impasto.git

Keywords: Deformation recovery · Soft tissue tracking · Computer-assisted intervention.

1 Introduction

Tissue deformation is common during laparoscopic intervention due to tool-tissue interaction and cardiac and respiratory pulsations. In this article, we define tissue deformation as time-variant surface structure and displacement. Besides, we also pay attention to the surface strain during the operation, an important biomechanical factor that indicates the tension status and may reveal

the tissue destruction mechanism [20, 21], for which continuous pointwise mapping and tracking are necessary. Various downstream applications, such as robot planning [24, 16, 18], intraoperative navigation [11, 23, 15] and surgical safety assessment [1, 3], may benefit from tissue deformation recovery, however, which remains challenging. The difficulties include, but are not limited to, complex tissue structure, camera motion, severe tissue deformation, and tool-tissue interaction that leads to surface change and occlusion.

Previous deformation recovery methods can be roughly divided into three categories: visual simultaneous localization and mapping (SLAM)-based [17, 14], neural field (NeF)-based [19, 22] and scene flow-based methods [2, 3]. SLAM has been widely used for reconstructing a large scale of a scene using images in an online approach. Recently, some have implemented SLAM-based techniques in reconstructing deformable scenes in the abdomen area [17, 14], but these methods are still vulnerable to severe tissue deformation and tool-induced occlusion and cannot cope with complex tissue structures [19]. NeF, as an implicit representation of 3D structure using multilayer perceptron (MLP), has been demonstrated to be useful in reconstructing 3D scenes with good characteristics for handling occlusion [13]. Recent NeF-based works succeeded in reconstructing surface deformation even in the occluded area from laparoscopic videos [19, 22]. However, the method is offline and suffers from its scene-specific characteristics, which hinder its application in continuous surface mapping. Moreover, neither the SLAM-based nor the NeF-based methods meet the requirement of continuous pointwise tracking, since SLAM-based methods typically perform the registration between the newly observed and the previously modeled scene in the point cloud scale [17, 14], while the NeF-based ones model the displacement, referring to a canonical space where the same entity may appear in multiple locations [13], leading to the failure of identifying the same entity in inter-frame tracking. On the other hand, scene flow models the pointwise inter-frame 3D displacement, which relies on the visibility of the points for tracking and thus is vulnerable to occlusion. To mitigate the occlusion problem, scene flow-based methods for tissue deformation recovery leverage thin-plate splines [3] or mesh connectivity [2] for interpolating the lost-of-tracking area. However, these methods hypothesize a constant surface continuity, which is not true in some operations like dissection, and cannot model points that move outside the field of view (FOV).

To overcome all these limitations, we propose a novel explicit representation of the deformation as the time-variant surface structure and displacement maps defined in a canonical canvas space. We then propose an online method for tissue deformation recovery by optimizing and fusing these maps based on the natural physical assumptions of spatiotemporal smoothness and visibility. The proposed method is robust to tool-induced occlusion and capable of continuous surface mapping and pointwise tracking under various operations, such as grasping, dissection, traction, and palpation, regardless of camera motion, as demonstrated via experiments using ex vivo and in vivo laparoscopic datasets.

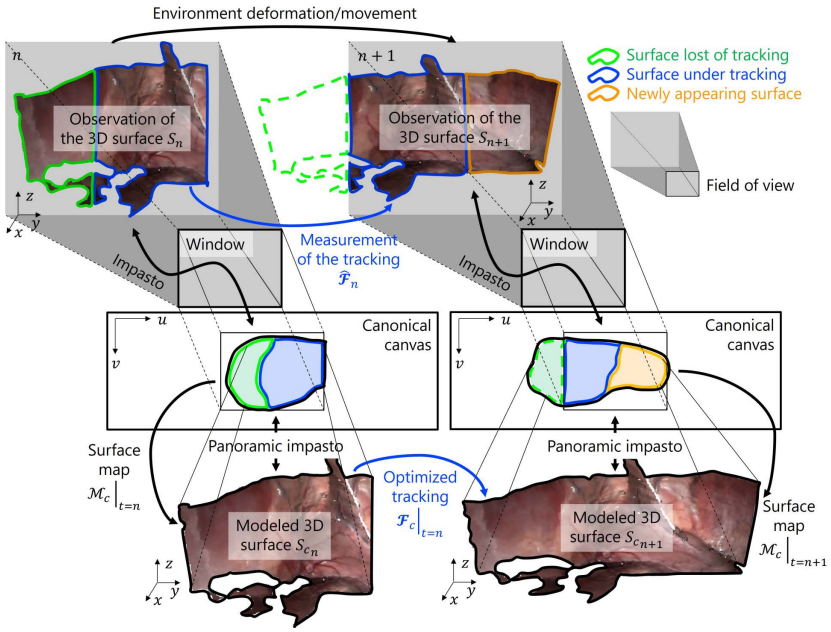

Fig. 1. Illustration of our proposed method, namely trans-window panoramic impasto, for online tissue deformation recovery.

2 Method

2.1 Overview

In this article, we propose an online method for deformation recovery from laparoscopic images. As shown in Fig. 1, an observer observes the environment through a window, representing the camera, and depicts the 3D structure on a canonical canvas as maps in a process named impasto. Although the observer is static to the window, since it leverages the currently and previously observed structure and tracks between these observations, it can depict a panoramic view of the outside environment just like the window does not exist. Such a novel problem setting is naturally suitable for handling a deforming environment, as it always models the latest status of the environment rather than modeling the environment under a rigid body assumption. Although some areas may have moved out of the FOV or be occluded, with the proposed optimization and fusion by preserving spatiotemporal smoothness and visibility, we can still recover their deformation in the sense of the time-variant surface structure and displacement.

2.2 Impasto: Parameterization of 3D Surface

We propose to leverage the surface map to represent the 3D surface of the tissues observed from the laparoscope, unlike previous methods [2, 17], where the

3D point cloud or the mesh were used. Inspired by impasto, a painting technique where paint is laid sticky on an area for stereoscopic feeling, we use the term impasto to describe the parameterization of a 3D surface on a 2D space. Let's say S is a 3D point set of a 3D surface. Impasto builds a surface map $\boldsymbol{\mathcal{M}}$ where each pixel corresponds to a 3D point, as $\boldsymbol{\mathcal{M}} : U \subset \mathbb{R}^2 \to S \subset \mathbb{R}^3$. In practice, we implement the camera projection to establish the correspondence between the pixels and 3D points. Although there is no limitation on the techniques for acquiring the 3D surface, we recommend implementing the binocular-based ones for better online performance [7, 8, 12]. Note that we only parameterize the smooth subsets of the 3D surface and neglect those rough areas like sharp edges and discontinuous areas. Such that $\boldsymbol{\mathcal{M}}$ is a homeomorphism and differentiable, meaning that $\boldsymbol{\mathcal{M}}$ has differential structure, which is useful in geometric optimization. The derivative of $\boldsymbol{\mathcal{M}}$ at $\boldsymbol{p} = (u, v) \in \mathbb{R}^2$ can be represented as:

$$d\boldsymbol{\mathcal{M}}|_p = \begin{bmatrix} \frac{\partial x}{\partial u} & \frac{\partial y}{\partial u} & \frac{\partial z}{\partial u} & \frac{\partial x}{\partial v} & \frac{\partial y}{\partial v} & \frac{\partial z}{\partial v} \end{bmatrix} \tag{1}$$

where $(x, y, z) = \boldsymbol{\mathcal{M}}(u, v)$. These derivative elements form tangent vectors and tangent planes of a 3D surface S at $\boldsymbol{\mathcal{M}}(\boldsymbol{p})$ [9], representing local geometric properties of the surface.

2.3 Canonical canvas

Unlike SLAM, where the camera is moving around the environment for gradually generating 3D mapping [17, 14], we propose a novel problem setting where an observer is static to the camera, the window, through which it performs impasto for the outside environment on a 2D space, namely the canonical canvas. The outside environment can be deforming and have relative motion with respect to the window, as shown in Fig. 1. As compared to the image space, where the height and the width are fixed, the canonical canvas is a borderless space that enables the impasto for the structure even outside the current FOV. Therefore, we can panoramically depict the environment in front of the observer while preserving its latest appearance and deformation status. In this article, the deformation is defined as time-variant surface structure and displacement. Thus, the canonical canvas is actually a space of $\mathbb{R}^2 \times t$.

2.4 Map Optimization

From the perspective of the observer, it is the environment that is moving rather than the camera. Such that we have a uniform representation of all the dynamic information, including the environment deformation and the rigid movement caused by camera motion, as a 3D displacement map (scene flow map) $\boldsymbol{\mathcal{F}}_c : U_c \subset \mathbb{R}^2 \to \mathbb{R}^3$ and a 2D displacement map (optical flow map) $\boldsymbol{\mathcal{O}}_c : U_c \subset \mathbb{R}^2 \to \mathbb{R}^2$ defined in the canonical canvas. These displacement maps indicate pointwise inter-frame tracking. However, in practice, due to occlusion, areas moving outside the FOV and the noise in the measurement of the tracking,

it is hardly possible to track the whole surface, as shown in Fig. 1. Note that the tool-induced occluded area, typically represented by the instrument mask, can be identified if the instrument pose is known [6] or using instrument segmentation [12]. Let's say $\widehat{\boldsymbol{\mathcal{F}}}_n : U_{c_{n_{\text{sub}}}} \subset \mathbb{R}^2 \rightarrow \mathbb{R}^3$ is a measured scene flow map from the n-th frame to the $(n+1)$-th frame and $\boldsymbol{\mathcal{M}}_c|_{t=n} : U_{c_n} \subset \mathbb{R}^2 \rightarrow S_{c_n} \subset \mathbb{R}^3$ is a surface map of the n-th frame, where $U_{c_{n_{\text{sub}}}} \subset U_{c_n}$ is the area in tracking, U_{c_n} is the whole area defined on the canonical canvas at the n-th frame, and S_{c_n} is the modeled 3D surface at the n-th frame. We want to estimate a surface map $\boldsymbol{\mathcal{G}}_n$ deforming from $\boldsymbol{\mathcal{M}}_c|_{t=n}$ that is consistent with the measured tracking, as:

$$\boldsymbol{\mathcal{G}}_n(\boldsymbol{p}) = \boldsymbol{\mathcal{M}}_c|_{t=n}(\boldsymbol{p}) + \widehat{\boldsymbol{\mathcal{F}}}_n(\boldsymbol{p}), \boldsymbol{p} \in U_{c_{n_{\text{sub}}}} \tag{2}$$

However, since there exists lost-of-tracking areas, the above estimation problem is ill-posed. We propose to introduce a spatiotemporal smoothness term for regularization by assuming that the local geometric properties represented by the derivatives of the reference map and the estimated map are similar, as:

$$d\boldsymbol{\mathcal{G}}_n|_p = \boldsymbol{\mathcal{R}}_n \left(d\boldsymbol{\mathcal{M}}_c|_{t=n,p} \right) \tag{3}$$

where $\boldsymbol{\mathcal{R}}_n$ is a rotation transformation estimated from $\widehat{\boldsymbol{\mathcal{F}}}_n$ using the method reported in [4], as $d\boldsymbol{\mathcal{M}}_c|_{t=n,p}$ is rotation-variant. With equation 2 and 3, we propose a map optimization model incorporating measured tracking and geometric smoothness, whose solution in the least squares sense is:

$$\begin{aligned} \widehat{\boldsymbol{\mathcal{G}}}_n = \arg\min_{\boldsymbol{\mathcal{G}}_n} & \left\| \int_{\boldsymbol{p} \in U_{c_{n_{\text{sub}}}}} \boldsymbol{\mathcal{G}}_n(\boldsymbol{p}) - \boldsymbol{\mathcal{M}}_c|_{t=n}(\boldsymbol{p}) - \widehat{\boldsymbol{\mathcal{F}}}_n(\boldsymbol{p}) \right\|^2 \\ & + \alpha \left\| \int_{\boldsymbol{p} \in U_{c_n}} d\boldsymbol{\mathcal{G}}_n|_p - \boldsymbol{\mathcal{R}}_n \left(d\boldsymbol{\mathcal{M}}|_{t=n,p} \right) \right\|^2 \end{aligned} \tag{4}$$

where α is a scalar weight, which can be empirically set to 1 and remains fixed in all the experiments, and $\widehat{\boldsymbol{\mathcal{G}}}_n$ is the estimated surface deformed from $\boldsymbol{\mathcal{M}}_c|_{t=n}$. Accordingly, we can calculate the optimized inter-frame pointwise scene flow $\boldsymbol{\mathcal{F}}_c|_{t=n} : U_{c_n} \subset \mathbb{R}^2 \rightarrow \mathbb{R}^3$ and the optical map $\boldsymbol{\mathcal{O}}_c|_{t=n} : U_{c_n} \subset \mathbb{R}^2 \rightarrow \mathbb{R}^2$.

2.5 Map Fusion

Given an estimated map $\widehat{\boldsymbol{\mathcal{G}}}_n : U_{c_n} \subset \mathbb{R}^2 \rightarrow S_{g_n} \subset \mathbb{R}^3$ deformed from the previous map $\boldsymbol{\mathcal{M}}_c|_{t=n}$ defined in the canonical canvas and a currently observable map within the FOV $\boldsymbol{\mathcal{M}}_{n+1} : U_{n+1} \subset \mathbb{R}^2 \rightarrow S_{n+1} \subset \mathbb{R}^3$, we want to fuse these two maps to depict newly appearing areas on the canonical canvas and to model the latest appearance and deformation of the environment. However, the estimated deformed surface S_{g_n} may not be fully visible to the observer due to self-folding or locating behind the canvas, even if the window does not exist. Therefore, pretending that the window does not exist, we perform panoramic impasto for

S_{g_n} to only keep the areas that are visible to the observer, resulting in a map $\boldsymbol{\mathcal{M}}_{g_n} : U_{g_n} \subset \mathbb{R}^2 \rightarrow S_{g_{n_{\text{sub}}}} \subset S_{g_n} \subset \mathbb{R}^3$. By fusing $\boldsymbol{\mathcal{M}}_{g_n}$ and $\boldsymbol{\mathcal{M}}_{n+1}$, we uniformly model the currently and previously observed 3D structure on the canonical canvas as $\boldsymbol{\mathcal{M}}_c|_{t=n+1} : (U_{g_n} \cup U_{n+1}) \subset \mathbb{R}^2 \rightarrow \left(S_{g_{n_{\text{sub}}}} \cup S_{n+1}\right) \subset \mathbb{R}^3$.

2.6 Surface Strain Estimation

Strain can be calculated from the relative changes of positions among points, for which continuous pointwise tracking is necessary. With the proposed method, we can easily compose the modeled optical flow map $\boldsymbol{\mathcal{O}}_c|_{t=n}$ and the surface map $\boldsymbol{\mathcal{M}}_c|_{t=n}$ for continuously tracking points of the 3D surface S_{c_a}, as:

$$\boldsymbol{\mathcal{M}}_{c_{a\rightarrow b}} = \boldsymbol{\mathcal{M}}_c|_{t=b} \circ \boldsymbol{\mathcal{O}}_c|_{t=b-dt} \circ ... \circ \boldsymbol{\mathcal{O}}_c|_{t=a} \tag{5}$$

where $\boldsymbol{\mathcal{M}}_{c_{a\rightarrow b}} : U_{c_a} \subset \mathbb{R}^2 \rightarrow S_{c_{a\rightarrow b}} \subset \mathbb{R}^3$ represents the tracking result from $t = a$ to $t = b$, and $S_{c_{a\rightarrow b}}$ is the tracked surface. Note that $S_{c_{a\rightarrow b}} \neq S_{c_b}$ as S_{c_b} may include some areas that do not exist at $t = a$. An accumulated scene flow map can be defined as:

$$\boldsymbol{\mathcal{F}}_{c_{a\rightarrow b}} = \boldsymbol{\mathcal{M}}_{c_{a\rightarrow b}} - \boldsymbol{\mathcal{M}}_c|_{t=a} : U_{c_a} \rightarrow \mathbb{R}^3 \tag{6}$$

Since $\boldsymbol{\mathcal{M}}_c|_{t=a}$ is a homeomorphism, its inverse $\boldsymbol{\mathcal{M}}_c^{-1}\big|_{t=a}$ exists. Then we can define a map from the 3D structure space to the 3D displacement space as:

$$\boldsymbol{\mathcal{K}} = \boldsymbol{\mathcal{F}}_{c_{a\rightarrow b}} \circ \boldsymbol{\mathcal{M}}_c^{-1}\big|_{t=a} : S_{c_a} \subset \mathbb{R}^3 \rightarrow \mathbb{R}^3 \tag{7}$$

$\boldsymbol{\mathcal{K}}$ is indeed a 3D displacement field. By applying the infinitesimal strain theory and the vertex-wise least-squares algorithm [2], we can calculate the surface strain using $\boldsymbol{\mathcal{K}}$.

3 Experiments

3.1 Datasets and Evaluation Metrics

We conducted experiments using ex vivo and in vivo binocular laparoscopic video datasets to evaluate the performance of the proposed method from various perspectives, including robustness to tool-induced occlusion, surface reconstruction accuracy in terms of the surface distance [2] in both occluded and non-occluded areas and the capability of estimating surface strain. We made use of two publicly available in vivo datasets, namely HAMLYN [10] and ENDONERF [19], and one ex vivo dataset taken by ourselves. HAMLYN and ENDONERF do not provide the ground truth of the 3D scene, while our ex vivo dataset utilizes the 3D scan results as the ground truth in both the occluded and non-occluded areas. These videos include various types of tool-tissue interaction (grasping, traction, dissection and palpation) and camera motion (large, small and none). Note that ENDONERF [19] provides the instrument masks directly and our ex vivo dataset provides the instrument poses in respect to the camera, such that the tool-induced occluded areas in both datasets can be easily identified.

3.2 Implementation Details

All the laparoscopic cameras in the datasets were calibrated, such that the images were rectified before processing. We followed the two-step approach in [2] to measure the 3D structure and tracking from the images. More specifically, we utilized the pre-trained models provided by RAFT-Stereo [8] for 3D reconstruction and LiteFlowNet3 [5] for 2D tracking and combined them for 3D tracking. These noisy measurements were processed by the proposed method in an online manner. The proposed method was implemented using MATLAB®. The code and the ex vivo dataset are available at: `https://github.com/bmpelab/trans_window_panoramic_impasto.git`.

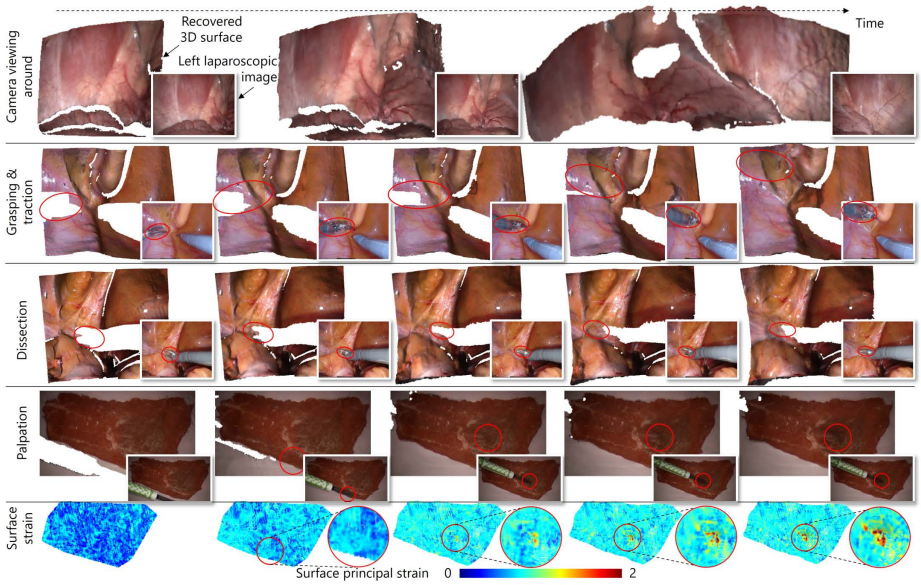

Fig. 2. Online deformation recovery results with the reference left laparoscopic images in the lower-right corner. Time increases from the left to the right. Red rings indicate the locations of the forceps. 1st row: camera moving around viewing the abdomen wall. 2nd-4th rows: various tool-tissue interaction cases, including grasping, traction, dissection and palpation. 5th row: surface strain during the palpation of the 4th row.

4 Results and Discussion

Figure 2 shows that the proposed method successfully recovers the tissue deformation in various cases, including the existence of large camera motion and various types of tool-tissue interaction (grasping, traction, dissection, palpation). Results in Fig. 2 demonstrate that the proposed method is robust to tool-induced

occlusion, as the structure and texture of the occluded tissue can still be recovered. We quantitatively compare the deformation recovery accuracy in terms of the surface distance among three methods: RAFT-Stereo [8], EndoSurf [22], and the proposed one. Note that RAFT-Stereo is a stereo matching algorithm implemented as a measurement of the 3D structure, whose results are used by EndoSurf and the proposed method. Thus, the error of RAFT-Stereo will be inherited. Besides, RAFT-Stereo is not robust to tool-induced occlusion. Therefore, its accuracy in the occluded areas is not available. As shown in Table 1, the surface distances of the proposed method in the occluded and non-occluded areas are 0.40 ± 0.26mm and 0.63 ± 0.63mm, respectively, and are lower than those of the EndoSurf, which are 8.19 ± 3.10mm and 2.26 ± 2.71mm, respectively, meaning that the proposed online method achieves higher reconstruction accuracy in both the occluded and non-occluded areas.

Table 1. Deformation recovery accuracy in terms of surface distance on our ex vivo dataset (unit in millimeter)

Surface distance in non-occluded areas (↓)			Surface distance in occluded areas (↓)		
RAFT-Stereo [8]	EndoSurf [22]	Ours	RAFT-Stereo [8]	EndoSurf [22]	Ours
0.39 ± 0.32	2.26 ± 2.71	0.63 ± 0.63	n.a.	8.19 ± 3.10	0.40 ± 0.26

As an online approach, the proposed method is designed for gradually modeling newly appearing surfaces. The first row of Fig.2 shows a case where the camera was moving around viewing the porcine abdomen wall, while the second row shows a case where the camera was fixed, one forceps were performing traction and the other was standing by. In both cases, those areas initially outside the FOV or occluded were modeled once they became visible to the camera. Therefore, the proposed method is capable of continuous mapping while maintaining the latest deformation status and appearance of the environment. Such that we overcome the limitations of the previous SLAM-based and NeF-based methods. However, the method is not for recovering the tissue in the permanently occluded areas. That is the reason why there remained some vacant areas in the final frames, as shown in Fig. 2, since these areas remained invisible to the camera.

The fifth row in Fig. 2 visualizes the principal surface strain during the palpation procedure in the fourth row. Though very noisy, we can identify that the strain increases as the forceps push deeper. The calculation of strain relies on the analysis of the relative changes of the locations of the neighboring points, for which continuously tracking surface points is necessary but non-trivial, especially with the existence of occlusion. Results in Fig. 2 demonstrate that the proposed method can handle such a challenging task and successfully bridge between the visual observation and surface biomechanical properties.

5 Conclusion

In this article, we propose an online method named trans-window panoramic impasto for surface deformation recovery from laparoscopic images. To realize continuous surface mapping and tracking and to handle tool-induced occlusion, we propose a novel problem setting where we assume a static observer depicts the deformable and movable environment outside a window (the camera) on a canonical canvas as surface and displacement maps. Based on such problem setting, we propose map-based optimization and fusion for estimating the occluded and outside FOV areas and modeling the newly appearing areas. Experiments using ex vivo and in vivo laparoscopic datasets were conducted. Results demonstrate that the proposed method successfully recovers tissue deformation in various cases with different types of tool-tissue interaction (grasping, palpation, traction, dissection) and camera motion with accuracy of 0.40 ± 0.26mm and 0.63 ± 0.63mm in the occluded and non-occluded areas, respectively.

Acknowledgments. This work was supported by JST Moonshot R&D Grant Number JPMJMS2214-02 and the Precision Measurement Technology Promotion Foundation (PMTP-F). Many thanks to Prof. Masamune (Institute of Advanced Biomedical Engineering and Science, Tokyo Women's Medical University, Tokyo, Japan) for advising the da Vinci vision system.

Disclosure of Interests. The authors have no competing interests to declare that are relevant to the content of this article.

References

1. Aviles, A.I., Alsaleh, S.M., Casals, A.: Sight to touch: 3D diffeomorphic deformation recovery with mixture components for perceiving forces in robotic-assisted surgery. In: 2017 IEEE/RSJ International Conference on Intelligent Robots and Systems (IROS). pp. 160–165 (2017)
2. Chen, J., Hara, K., Kobayashi, E., Sakuma, I., Tomii, N.: Occlusion-robust scene flow-based tissue deformation recovery incorporating a mesh optimization model. International Journal of Computer Assisted Radiology and Surgery **18**(6), 1043–1051 (2023)
3. Giannarou, S., Ye, M., Gras, G., Leibrandt, K., Marcus, H.J., Yang, G.Z.: Vision-based deformation recovery for intraoperative force estimation of tool–tissue interaction for neurosurgery. International Journal of Computer Assisted Radiology and Surgery **11**(6), 929–936 (2016)
4. Horn, B.K.P.: Closed-form solution of absolute orientation using unit quaternions. JOSA A **4**(4), 629–642 (1987)
5. Hui, T.W., Loy, C.C.: LiteFlowNet3: Resolving Correspondence Ambiguity for More Accurate Optical Flow Estimation. In: Vedaldi, A., Bischof, H., Brox, T., Frahm, J.M. (eds.) Computer Vision – ECCV 2020. pp. 169–184. Lecture Notes in Computer Science, Springer International Publishing, Cham (2020)
6. Li, Y., Richter, F., Lu, J., Funk, E.K., Orosco, R.K., Zhu, J., Yip, M.C.: SuPer: A Surgical Perception Framework for Endoscopic Tissue Manipulation With Surgical Robotics. IEEE Robot. Autom. Lett. **5**(2), 2294–2301 (Apr 2020)

7. Li, Z., Liu, X., Drenkow, N., Ding, A., Creighton, F.X., Taylor, R.H., Unberath, M.: Revisiting Stereo Depth Estimation From a Sequence-to-Sequence Perspective With Transformers. In: Proceedings of the IEEE/CVF International Conference on Computer Vision. pp. 6197–6206 (2021)
8. Lipson, L., Teed, Z., Deng, J.: RAFT-Stereo: Multilevel Recurrent Field Transforms for Stereo Matching. In: 2021 International Conference on 3D Vision (3DV). pp. 218–227. IEEE Computer Society (2021)
9. Manfredo, C.: Differential Geometry of Curves and Surfaces. 2 edn. (2016)
10. Mountney, P., Stoyanov, D., Yang, G.Z.: Three-Dimensional Tissue Deformation Recovery and Tracking. IEEE Signal Processing Magazine **27**(4), 14–24 (2010)
11. Pelanis, E., Teatini, A., Eigl, B., Regensburger, A., Alzaga, A., Kumar, R.P., Rudolph, T., Aghayan, D.L., Riediger, C., Kvarnström, N., Elle, O.J., Edwin, B.: Evaluation of a novel navigation platform for laparoscopic liver surgery with organ deformation compensation using injected fiducials. Medical Image Analysis **69**, 101946 (2021)
12. Psychogyios, D., Mazomenos, E., Vasconcelos, F., Stoyanov, D.: MSDESIS: Multitask Stereo Disparity Estimation and Surgical Instrument Segmentation. IEEE Transactions on Medical Imaging **41**(11), 3218–3230 (2022)
13. Pumarola, A., Corona, E., Pons-Moll, G., Moreno-Noguer, F.: D-NeRF: Neural Radiance Fields for Dynamic Scenes. In: 2021 IEEE/CVF Conference on Computer Vision and Pattern Recognition (CVPR). pp. 10313–10322. IEEE, Nashville, TN, USA (2021)
14. Recasens, D., Lamarca, J., Facil, J.M., Montiel, J.M.M., Civera, J.: Endo-Depth-and-Motion: Reconstruction and Tracking in Endoscopic Videos Using Depth Networks and Photometric Constraints. IEEE Robotics and Automation Letters **6**(4), 7225–7232 (2021)
15. Schneider, C., Allam, M., Stoyanov, D., Hawkes, D.J., Gurusamy, K., Davidson, B.R.: Performance of image guided navigation in laparoscopic liver surgery – A systematic review. Surgical Oncology **38**, 101637 (2021)
16. Shin, C., Ferguson, P.W., Pedram, S.A., Ma, J., Dutson, E.P., Rosen, J.: Autonomous Tissue Manipulation via Surgical Robot Using Learning Based Model Predictive Control. In: 2019 International Conference on Robotics and Automation (ICRA). pp. 3875–3881 (2019)
17. Song, J., Wang, J., Zhao, L., Huang, S., Dissanayake, G.: MIS-SLAM: Real-Time Large-Scale Dense Deformable SLAM System in Minimal Invasive Surgery Based on Heterogeneous Computing. IEEE Robotics and Automation Letters **3**(4), 4068–4075 (2018)
18. Tagliabue, E., Pore, A., Dall'Alba, D., Magnabosco, E., Piccinelli, M., Fiorini, P.: Soft Tissue Simulation Environment to Learn Manipulation Tasks in Autonomous Robotic Surgery. In: 2020 IEEE/RSJ International Conference on Intelligent Robots and Systems (IROS). pp. 3261–3266 (2020)
19. Wang, Y., Long, Y., Fan, S.H., Dou, Q.: Neural Rendering for Stereo 3D Reconstruction of Deformable Tissues in Robotic Surgery. In: Wang, L., Dou, Q., Fletcher, P.T., Speidel, S., Li, S. (eds.) Medical Image Computing and Computer Assisted Intervention – MICCAI 2022. pp. 431–441. Lecture Notes in Computer Science, Springer Nature Switzerland, Cham (2022)
20. Yamamoto, K., Hara, K., Kobayashi, E., Akagi, Y., Sakuma, I.: Tissue damage force estimation in porcine small intestine from its elasticity. International Journal of Computer Assisted Radiology and Surgery **18**(3), 587–594 (2023)

21. Yamamoto, K., Hara, K., Kobayashi, E., Yuki, A., Sakuma, I.: Tissue histology on the correlation between fracture energy and elasticity. International Journal of Computer Assisted Radiology and Surgery (2023)
22. Zha, R., Cheng, X., Li, H., Harandi, M., Ge, Z.: EndoSurf: Neural Surface Reconstruction of Deformable Tissues with Stereo Endoscope Videos. In: Greenspan, H., Madabhushi, A., Mousavi, P., Salcudean, S., Duncan, J., Syeda-Mahmood, T., Taylor, R. (eds.) Medical Image Computing and Computer Assisted Intervention – MICCAI 2023. pp. 13–23. Lecture Notes in Computer Science, Springer Nature Switzerland, Cham (2023)
23. Zhang, X., Ji, X., Wang, J., Fan, Y., Tao, C.: Renal surface reconstruction and segmentation for image-guided surgical navigation of laparoscopic partial nephrectomy. Biomedical Engineering Letters **13**(2), 165–174 (2023)
24. Zhu, J., Cherubini, A., Dune, C., Navarro-Alarcon, D., Alambeigi, F., Berenson, D., Ficuciello, F., Harada, K., Kober, J., Li, X., Pan, J., Yuan, W., Gienger, M.: Challenges and Outlook in Robotic Manipulation of Deformable Objects. IEEE Robotics & Automation Magazine **29**(3), 67–77 (2022)